ACS NANO

www.acsnano.org

ARTICLE

A Carbonyl and Azo-Based Polymer Cathode for Low-Temperature Na-Ion Batteries

Eric Youngsam Kim, Motahareh Mohammadiroudbari, Fu Chen, Zhenzhen Yang, and Chao Luo*

Cite This: https://doi.org/10.1021/acsnano.3c08860

Read Online

ACCESS | Metrics & More | Article Recommendations | Supporting Information

ABSTRACT: Due to flexible structure tunability and abundant structure diversity, redox-active polymers are promising cathode materials for developing affordable and sustainable Na-ion batteries (NIBs). However, polymer cathodes still suffer from low capacity, poor cycle life, and sluggish reaction kinetics. Herein, we designed and synthesized a polymer cathode material bearing carbonyl and azo groups as well as extended conjugation structures in the repeating units. The polymer cathode exhibited exceptional electrochemical performance in NIBs in terms of high capacity, long lifetime, and fast kinetics. When coupled with a low-concentration electrolyte, it shows superior performance at low temperatures down to −50 °C, demonstrating great promise for low-temperature battery applications. Raman spectroscopy, X-ray photoelectron spectroscopy (XPS), and scanning electron microscopy (SEM) were employed to study the reaction mechanism, interphase structure, and morphological evolution, confirming reversible redox reactions between azo/carbonyl groups in the polymer and Na^+/electrons, a NaF-rich interphase, and high structure stability upon cycling. This work provides an effective approach to developing high-performance polymer cathodes for affordable, sustainable, and low-temperature NIBs.

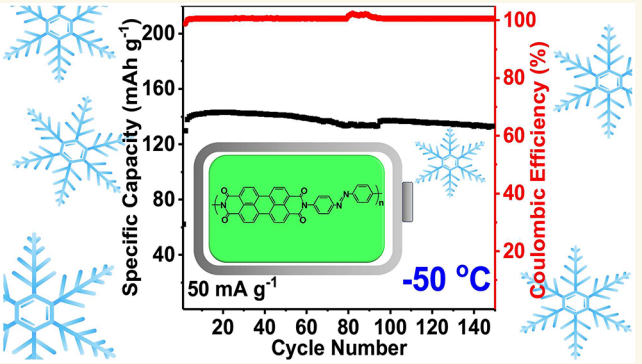

KEYWORDS: *Redox-active polymer, cathode, Na-ion batteries, low-temperature batteries, low-concentration electrolyte, carbonyl group, azo group*

Lithium-ion batteries (LIBs) are dominant energy storage devices in portable electronics, electric vehicles, and grid-scale energy storage due to their high capacity and long cycle life.[1−3] However, commercial LIBs, consisting of graphite-based anodes and transition-metal-oxide-based cathodes, face challenges such as the high toxicity of cobalt resources, the high cost of lithium, and the scarcity of certain transition metals. To overcome these challenges, significant research efforts have been devoted to exploring advanced materials and chemistries to replace conventional LIB chemistry for next-generation sustainable energy storage systems.[4−7] Among various battery chemistries, Na-ion batteries (NIBs) are promising because of low cost and abundance of sodium resources, as well as similar redox chemistries of NIBs with LIBs.[8−10] Therefore, the development of high-performance, affordable, and sustainable NIBs is paramount.

To date, the cathode continues to be a limiting factor for the development and application of NIBs, presenting major challenges. Among various NIB cathodes, layered transition metal oxides attract significant research interests because they have similar properties as layered lithium transition metal oxides such as high theoretical specific capacity and high redox potentials.[11−15] Additionally, Prussian blue analogues are also promising cathodes for NIBs because of their low cost, high theoretical capacity, facile synthesis methods, and environmental benignity. However, most layered transition-metal-oxide-based cathodes in NIBs suffer from time- and energy-consuming synthetic processes and have a moderate cycle life caused by structural degradation, while the presence of interstitial water molecules and defects in Prussian blue analogue channels blocks Na-ion insertion, resulting in reduced capacity, short lifespan, and slow reaction kinetics.[16−19] Therefore, developing high-performance cathodes for NIBs is vital to achieving next-generation sustainable energy storage systems.

Received: September 15, 2023
Revised: January 19, 2024
Accepted: January 22, 2024

Scheme 1. (a) Synthetic Procedure of PTAD; (b) Proposed Reaction Mechanism of the PTAD Cathode, Where M Represents Na/K

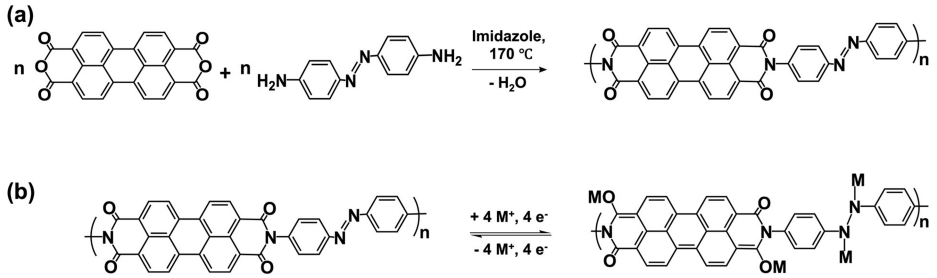

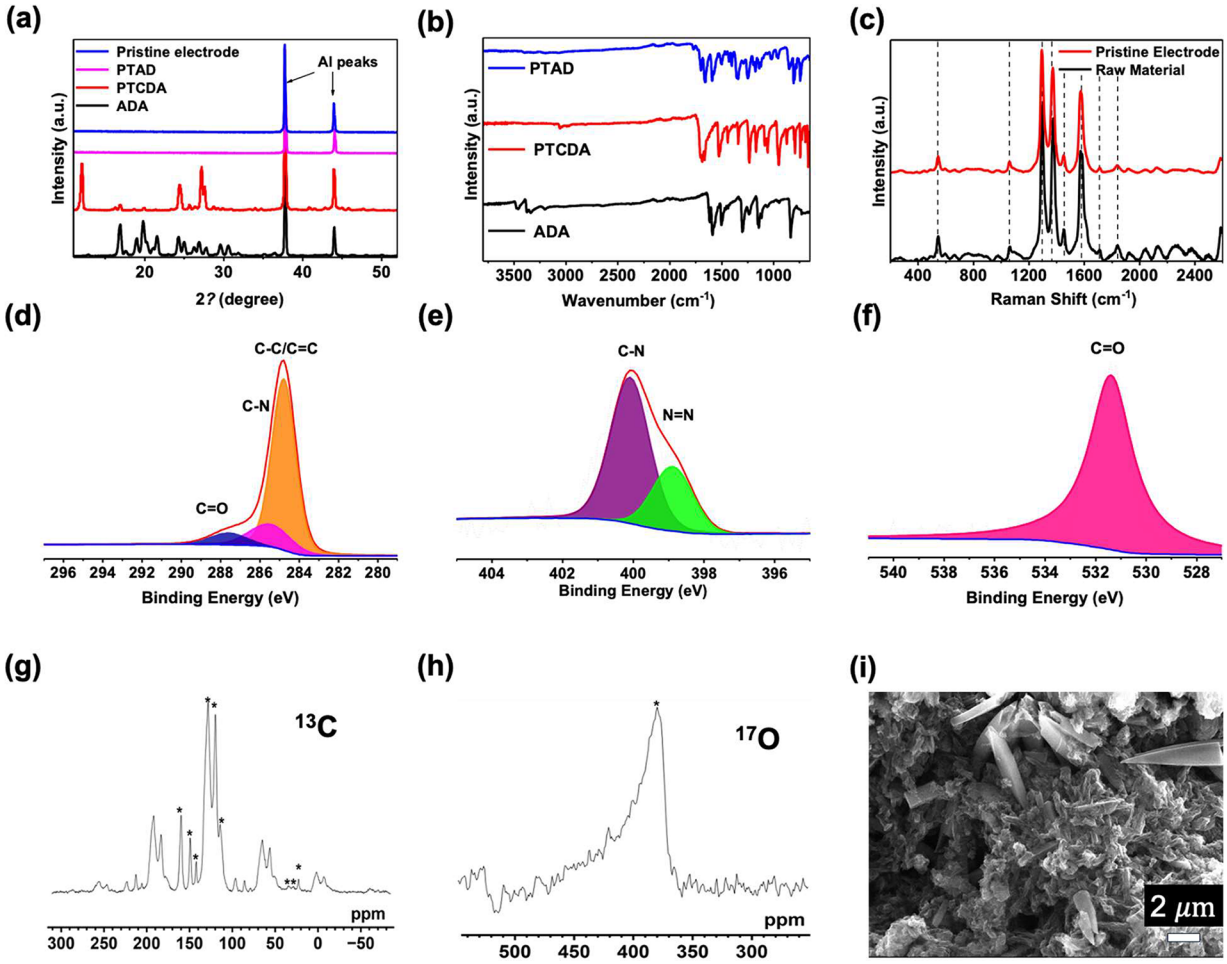

Figure 1. Material characterizations for PTAD and the PTAD-NGr composite: (a) XRD patterns; (b) FT-IR spectra; (c) Raman spectra of PTAD and its pristine electrode; (d) C 1s, (e) N 1s, (f) O 1s XPS spectra for PTAD; (g) ^{13}C, (h)^{17}O solid-state NMR (note, peaks with * indicate isotropic chemical shifts, and the other peaks without * are magic-angle spinning sidebands); (i) SEM image for PTAD.

In addition, low-temperature applications of rechargeable batteries have been surging because of ever-increasing exploration in polar regions and outer space. However, the performance of state-of-the-art batteries cannot satisfy the requirements for low-temperature batteries.[20,21] In this regard, the higher reactivity of sodium compared to lithium facilitates reaction kinetics, enabling the development of low-temperature NIBs. The design and synthesis of advanced materials and electrolytes are essential for achieving high-performance NIBs at low temperatures.[22−24] To this end, all of the components in NIBs need to be researched to optimize the electrochemical performance. For example, a low-concentration electrolyte with low viscosity and high ionic conductivity was designed to enable low-temperature NIBs.[25−27] Further performance optimization is also dependent on advanced cathode materials.

Among various cathode materials, organic small molecules and polymers stand out due to their lightweight, low cost, abundance, high sustainability, and flexible tunability. Various redox-active functional groups, such as carbonyl (C═O), imine (C═N), thioester (C═S), azo (N═N), and free radicals, have been designed into organic electrode materials to store sodium ions. However, challenges such as low conductivity, high solubility in the electrolyte, and significant volume change during the sodiation/desodiation process impede the development of organic NIBs.[28] To address these challenges, carbon coating, salination, polymerization,

https://doi.org/10.1021/acsnano.3c08860
ACS Nano XXXX, XXX, XXX−XXX

etc. have been applied. Among these methods, polymerization is promising due to the flexible structure, high stability, and negligible solubility of polymers. Incorporating multiple functional groups and extended conjugation structures into the repeating units of redox-active polymers can enhance the electrochemical performance, resulting in high capacity, a long lifetime, and fast kinetics. However, the correlation between the structure and performance remains elusive. Furthermore, the performance of redox-active polymers in low-temperature NIBs is of significant interest, but it remains largely unexplored.

Herein, we designed a polymer cathode material consisting of azo and carbonyl groups along with extended conjugated structures in the repeating units. This polymer was synthesized through a polycondensation method employing perylenetetracarboxylic dianhydride (PTCDA) and 4,4′-azodianiline (ADA) monomers. The synthetic procedure and proposed reaction mechanism of the polymer product (PTAD) are illustrated in Scheme 1a and b, respectively. The structure and morphology of PTAD were confirmed by using various techniques, including X-ray diffraction (XRD), Fourier-transform infrared spectroscopy (FTIR), Raman spectroscopy, solid-state nuclear magnetic resonance (NMR), X-ray photoelectron spectroscopy (XPS), and scanning electron microscopy (SEM). To enhance cathode conductivity and stability, nitrogen-doped single-layer graphene (NGr) was employed as an additive in the cathode to facilitate $\pi-\pi$ stacking between the conjugation structures in graphene and PTAD. The PTAD cathode exhibits high reversible capacity (206.8 mAh g^{-1} at 50 mA g^{-1}), long cycle life (1,500 cycle), and fast rate capability (up to 10 A g^{-1}) in NIBs at room temperature. When coupled with a low-concentration electrolyte, it demonstrates superior performance in terms of high capacity and high stability at temperatures as low as −50 °C, illustrating great promise for low-temperature applications. The reaction mechanism, interphase structure, and morphology evolution were studied using Raman spectroscopy, XPS, and SEM, confirming the reversible redox reactions between azo/carbonyl groups in the polymer and Na^+/electrons, as well as the presence of a NaF-rich interphase and high structural stability upon cycling. Therefore, the PTAD polymer represents a promising cathode material for affordable, sustainable, and low-temperature NIBs.

RESULTS/DISCUSSION

To confirm molecular, crystalline, and morphological structures of PTAD, we employed FTIR, Raman spectroscopy, XRD, XPS, solid-state NMR, and SEM. In the XRD patterns (Figure 1a), PTCDA and ADA monomers exhibit sharp peaks in the range from 10 to 32°, while PTAD does not show any peaks in the XRD spectra, indicating an amorphous structure. In the FTIR (Figure 1b), intense peaks were detected at 1688 and 1684 cm^{-1}, representing the stretching vibration of the carbonyl (C═O) group in PTCDA and PTAD, respectively. The FTIR spectra of ADA and PTCDA also exhibited the stretching vibration of the azo group (N═N) at 1502 and 1498 cm^{-1}. Additionally, absorption peaks at 1142 and 1135 cm^{-1} indicated C−N stretching in ADA and PTAD. For the ADA monomer, absorption peaks at 3455 and 3369 cm^{-1} were induced by N−H stretching from the $-NH_2$ group.[29,30] However, N−H stretching peaks were not observed in PTAD, demonstrating the conversion of $N-H_2$ to imide through the condensation reaction. The Raman spectra of PTAD and the pristine electrode are shown in Figure 1c. The Raman peaks at 1063.5, 1308, and 1380.7 cm^{-1} indicate the stretching vibration of the azo group.[31] The carbonyl vibration induces a peak at 1578.13 cm^{-1} (Figure 1c). The pristine PTAD electrode exhibits Raman peaks similar to those of the PTAD powder. XPS was further employed to study the structure of PTAD. As shown in Figure 1d−f, XPS spectra of PTAD exhibit elemental composition with peaks corresponding to C 1s, N 1s, and O 1s. In the C 1s spectrum, three peaks were observed at 284.8, 285.6, and 287.7 eV, indicating C−C/C═C, C−N, and C═O, respectively. The C 1s peak at 284.8 eV is the reference peak for XPS. In the N 1s spectrum, two peaks at 400.1 eV for graphitic-N and 399.0 eV for N═N were detected. In O 1s spectrum, only one carbonyl peak was observed at 531.2 eV. The XPS results are well matched with the molecular structure of PTAD. Since PTAD is insoluble in organic solvents, solid-state NMR was performed to confirm the molecular structure (Figure 1g,h). In the ^{13}C NMR spectrum, the peak at 160 ppm indicates carbon from the carbonyl group. The peak at 150 ppm corresponds to the aromatic carbons bonding with C−N, while the four peaks at 110−140 ppm stand for the other aromatic carbon bonds in the benzene rings. In ^{17}O NMR spectrum, the single strong peak at 380 ppm originates from the oxygen of carbonyl groups in PTAD.[29,32] To measure the molecular weight of PTAD, it must be dissolved in dimethylformamide (DMF) or tetrahydrofuran (THF) solvents for the gel permeation chromatography test. However, PTAD did not dissolve in either dimethylformamide (DMF) or tetrahydrofuran (THF) solvents. DMF was used to purify the PTAD product and wash away the impurities, while PTAD does not dissolve in THF as evidenced in Figure S1. The morphology of PTAD was analyzed by SEM, which shows the irregular shape of microsized PTAD particles (Figure 1i). Therefore, the material characterization results confirm the molecular, amorphous, and microsized structures of PTAD.

The electrochemical performance of the PTAD electrode was evaluated in NIBs using 0.5 M $NaPF_6$ in diethylene glycol dimethyl ether (DEGDME) electrolyte, which is appropriate for both room-temperature and low-temperature battery tests. To determine the appropriate concentration of $NaPF_6$ in the electrolyte, we conducted a freezing test on electrolytes with different concentrations ranging from 0.5 to 1.0 M (Figure S2). These electrolytes were placed in a low-temperature chamber at −50 °C for 24 h. Frozen solids were observed in the electrolytes with concentrations ranging from 0.6 to 1.0 M, while only 0.5 M $NaPF_6$ in the DEGDME electrolyte remained as a clear solution. To further assess the electrochemical stability window of this electrolyte, a cyclic voltammetry (CV) test (Figure S3) at a scan rate of 2.0 mV s^{-1} was employed. The CV diagram showed a pair of redox peaks centered at 0 V, indicating plating and striping of the Na metal anode. No additional peaks were observed in the voltage range from 0 to 3.5 V, demonstrating that the 0.5 M $NaPF_6$ in the DEGDME electrolyte is stable and suitable for evaluating the performance of the PTAD cathode. We conducted solubility tests for the PTAD cathode and powder in various solvents and the electrolyte. To verify the solubility, UV-light spectroscopy was also employed. Each cathode was immersed in 3 mL of DEGDME solvent and 0.5 M $NaPF_6$ DEGDME electrolyte as shown in Figure S4. The color of pristine PTAD is dark red, but there is no color change after PTAD cathodes were added to the solvent or electrolyte at the beginning and overnight, demonstrating that PTAD is insoluble in DEGDME or the electrolyte. To further confirm this, these solutions were

https://doi.org/10.1021/acsnano.3c08860
ACS Nano XXXX, XXX, XXX−XXX

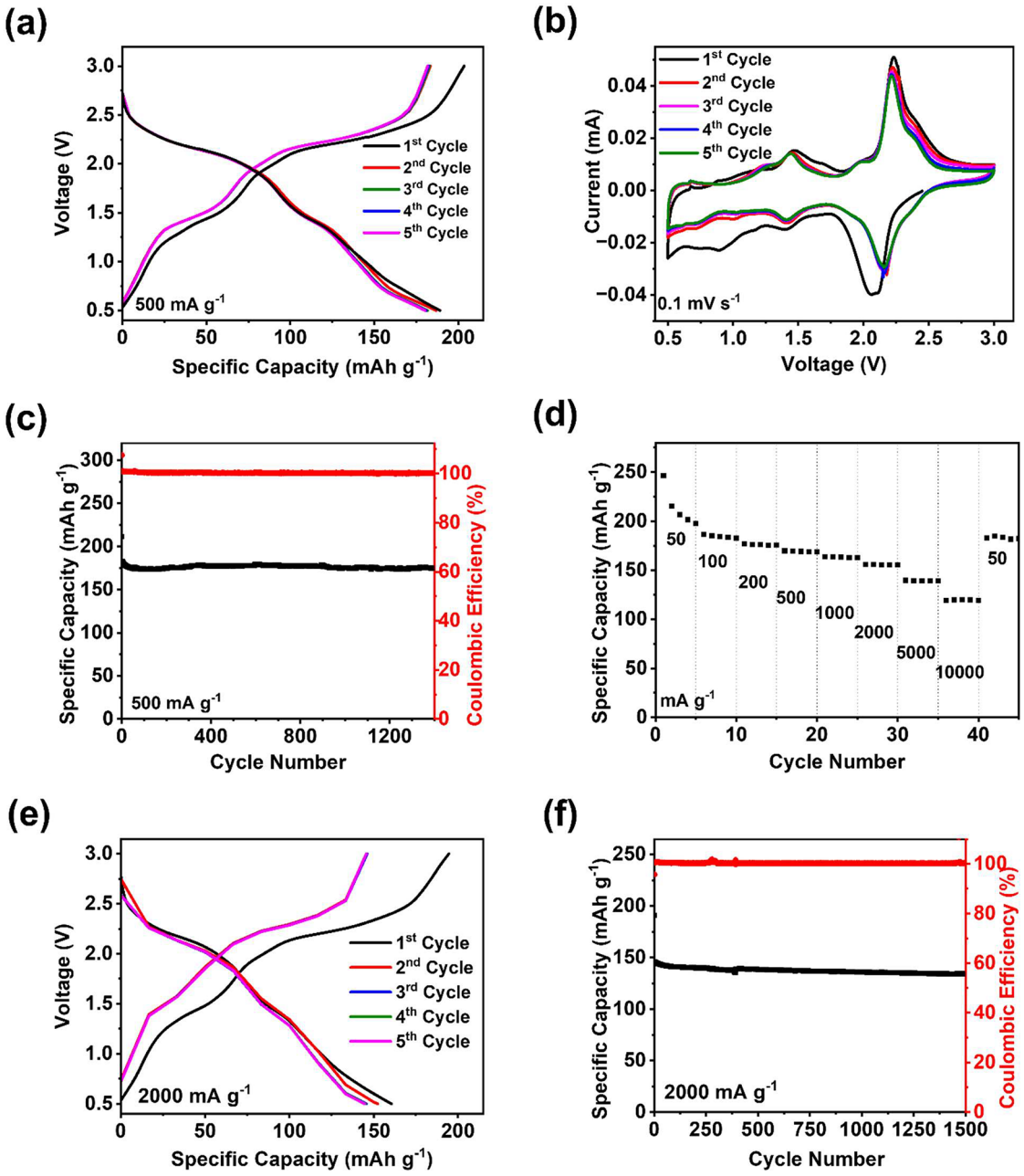

Figure 2. Electrochemical performances of the PTAD cathode in NIBs. (a) Galvanostatic charge−discharge curves at 500 mA g^{-1}; (b) cyclic voltammograms at 0.1 mV s^{-1}; (c) specific capacity and Coulombic efficiency versus cycle number at 500 mA g^{-1}; (d) rate capability at various current densities; (e) galvanostatic charge−discharge curves at 2000 mA g^{-1}; (f) charge capacity and Coulombic efficiency versus cycle number at 2000 mA g^{-1}.

measured by UV−vis spectroscopy tests. As shown in Figure S4c and f, no absorption peak was detected from the solutions, confirming the insolubility of PTAD in the solvent and electrolyte. Subsequently, further electrochemical measurements were carried out in this low-concentration electrolyte at room and low temperatures.

The electrochemical performance of the PTAD cathode in NIBs was measured within the voltage cutoff window of 0.5−3.0 V. The galvanostatic charge−discharge curves are shown in Figure 2a. The PTAD cathode delivered an initial capacity of 211.33 mAh g^{-1} at 500 mA g^{-1} with four pairs of sloping redox plateaus centered at 1.1, 1.4, 2.0, and 2.2 V for the azo reaction and carbonyl reaction, respectively. There are two electrochemically active sites in PTAD, which are carbonyl and azo groups. The low discharge plateau at ∼1.5 V is caused by the redox reaction between azo groups and Na ions, while carbonyl groups react with Na ions at ∼2.2 V. To enhance the average discharge voltage of the PTAD||Na cell, more carbonyl groups and some electron-withdrawing functional groups can be introduced into PTAD. In the CV test (Figure 2b) at a scan rate of 0.1 mV s^{-1}, four cathodic peaks at 1.0, 1.4, 1.9, and 2.1 V and four anodic peaks at 1.2, 1.4, 2.0, and 2.2 V were observed. These correspond to the redox plateaus observed in the galvanostatic charge−discharge curves. The redox peaks at 1.9/2.0 V and 2.2/2.3 V correspond to sodiation/desodiation of the carbonyl groups, while the redox peaks at 1.0/1.24 V and 1.4/1.4 V correspond to sodiation/desodiation of the azo groups. In the long term cycling tests, PTAD retained 83% of

https://doi.org/10.1021/acsnano.3c08860
ACS Nano XXXX, XXX, XXX−XXX

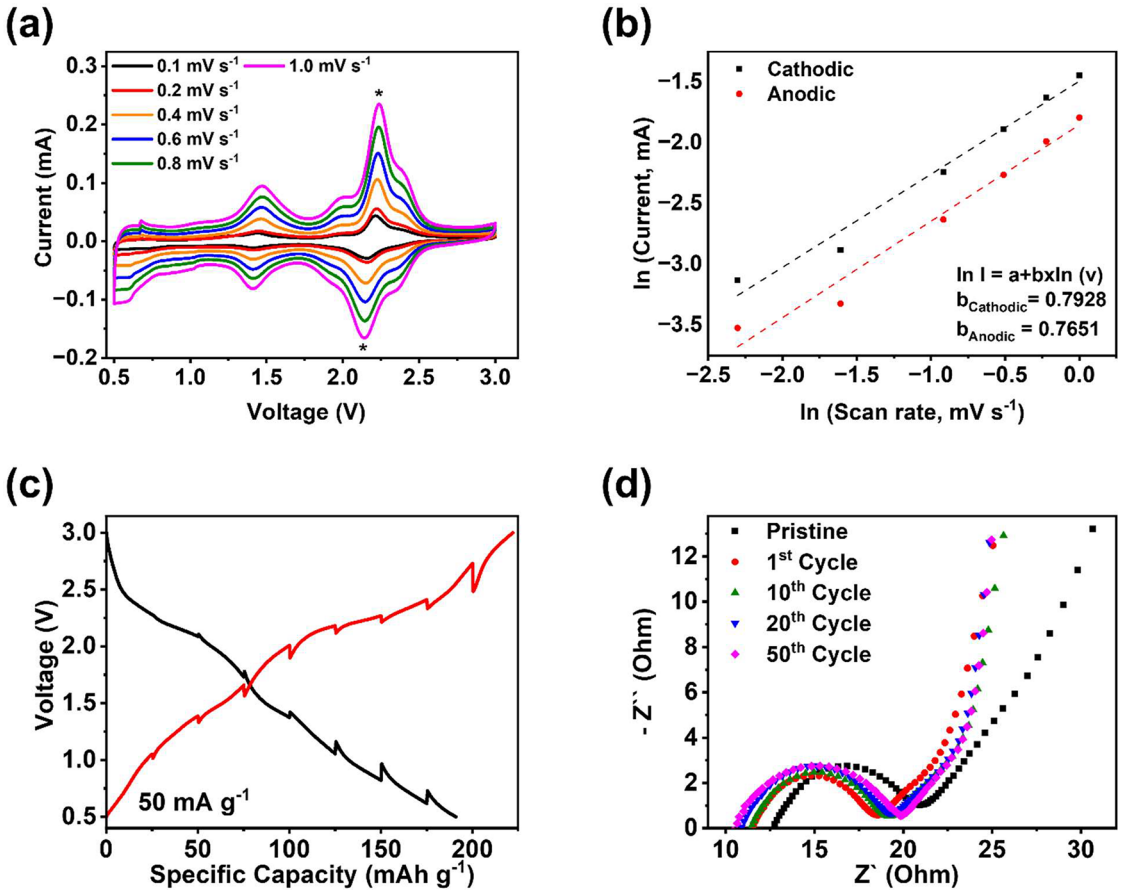

Figure 3. Kinetics study of the PTAD cathode. (a) Cyclic voltammograms at various scan rates from 0.1 to 1.0 mV s^{-1}; (b) Randles−Sevick plot of peak currents versus scan rates; (c) potential responses of GITT measurement; (d) impedance analysis for pristine and cycled PTAD cathodes.

its initial specific capacity (174.7 mAh g^{-1}), with high coulombic efficiency close to 100% after 1400 cycles (Figure 2c), demonstrating a very slow capacity decay rate of 0.012% per cycle. To exclude the capacity contribution from NGr, we prepared two electrodes: the PTAD cathode without NGr and the graphene electrode. The PTAD cathode without NGr was prepared using PTAD, carbon black, and sodium alginate (SA) in a mass ratio of 8:1:1. The graphene electrode was prepared by using NGr, carbon black, and SA with a mass ratio of 8:1:1. The cycling tests were conducted at room temperature with a current density of 500 mA g^{-1}. As shown in Figure S5a,b, the initial specific capacity of the pure PTAD cathode was 136.6 mAh g^{-1}. It was reduced to 101.1 mAh g^{-1} in the second cycle, and then the pure PTAD cathode delivered a stable cycle life of 500 cycles. The graphene electrode exhibited an initial capacity of 32.4 mAh g^{-1} and a stable cycle life of 100 cycles (Figure S5c,d). The $\pi-\pi$ stacking between NGr and PTAD, caused by the overlap between conjugation structures in NGr and PTAD, contributes to the superior performance of the PTAD cathode. It improves the conductivity and stability of the PTAD cathode. To provide evidence of $\pi-\pi$ stacking between NGr and PTAD, we compared the performance of the PTAD cathode with NGr to that of the PTAD cathode without NGr and the graphene electrode. As shown in Figures 2 and S5, the PTAD cathode with NGr outperforms the PTAD cathode without NGr and the graphene electrode in terms of high reversible capacity and a long cycle life. Though there was an extra 20% NGr in the PTAD cathode compared to the PTAD cathode without NGr, the capacity of the PTAD cathode with NGr is higher than the sum of the capacities of the PTAD cathode without NGr and the graphene electrode. The improved electrochemical performance is attributed to $\pi-\pi$ stacking between PTAD and NGr.[41] To further prove $\pi-\pi$ stacking, CV was employed to compare the PTAD cathodes with and without NGr. The content of carbon black in the PTAD cathode without NGr for the CV test was enhanced to 30 wt %. As shown in Figure S6, the redox peaks of the PTAD cathode with NGr are much stronger than those of the PTAD cathode without NGr, confirming that $\pi-\pi$ stacking between PTAD and NGr enhances the electrochemical performance of the PTAD cathode.[42,43] Since the PTAD cathode with NGr exhibited the best performance among the three electrodes, it was used for further tests. The rate performance of the PTAD cathode at room temperature is depicted in Figure 2d, where specific capacities of 206.7, 184.2, 176, 169.2, 163.3, 155.6, 139, and 119.8 mAh g^{-1} were obtained at different current densities of 50, 100, 200, 500, 1000, 2000, 5000, and 10 000 mA g^{-1}. After cycling at 10 000 mA g^{-1}, the current density was returned to 50 mA g^{-1}, and the specific capacity was immediately recovered to 183.5 mA g^{-1} (Figure 2d), indicating robust reaction kinetics. Consequently, the PTAD cathode was further cycled at a high current density of 2000 mA g^{-1}. The initial specific capacity was 191.4 mA g^{-1}, and it was retained at 134 mAh g^{-1} after 1500 cycles (Figure 2e,f), demonstrating high cyclic stability and fast charging capability.

https://doi.org/10.1021/acsnano.3c08860
ACS Nano XXXX, XXX, XXX−XXX

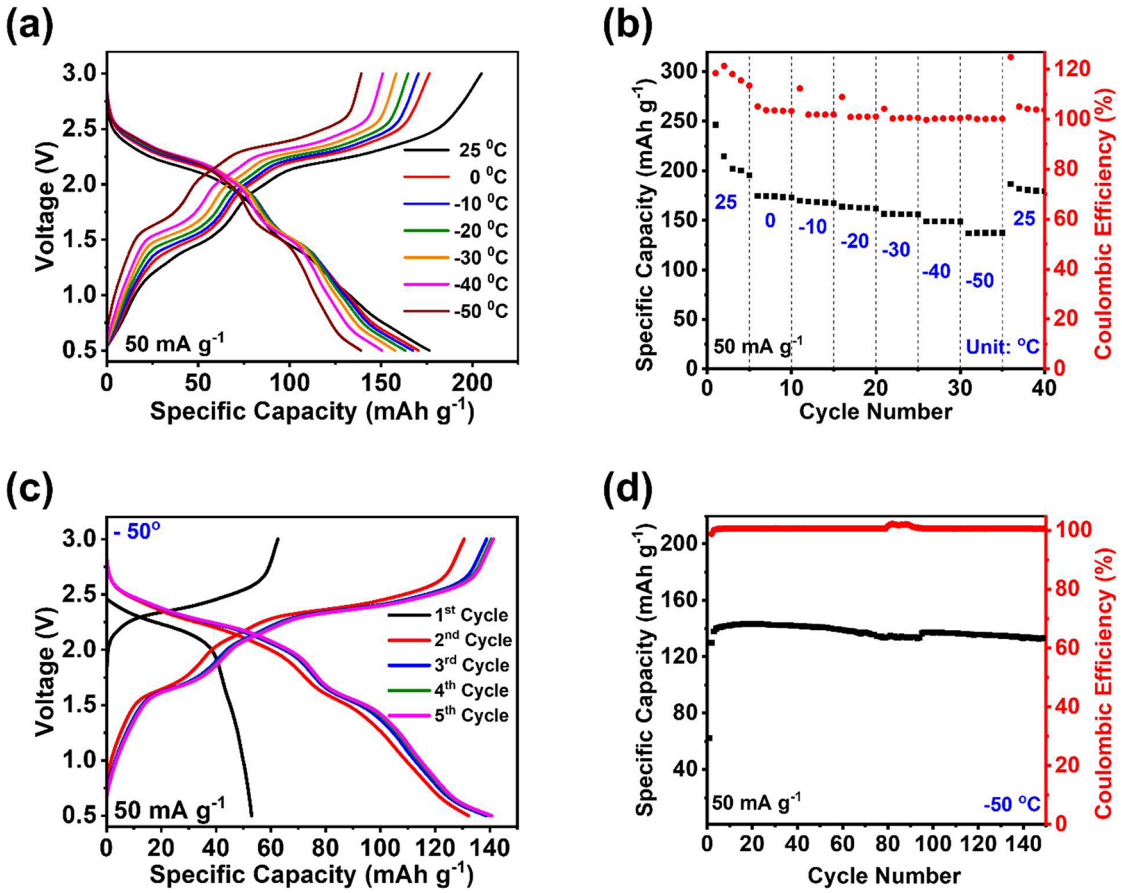

Figure 4. Low-temperature performance of the PTAD cathode. (a) Galvanostatic charge−discharge curves at 50 mA g^{-1} and various temperature; (b) rate capability at 50 mA g^{-1} and various temperatures; (c) galvanostatic charge−discharge curves at 50 mA g^{-1} and −50 °C; (d) specific capacity and coulombic efficiency versus cycle number at 50 mA g^{-1} and −50 °C.

Since the PTAD cathode exhibited exceptional performance in NIBs, its electrochemical performance was also measured in K-ion batteries (KIBs). The performance of PTAD in KIBs was tested in the cutoff window of 1.0−2.9 V. The PTAD cathode delivered an initial capacity of 172.5 mAh g^{-1} at 50 mA g^{-1} (Figure S7a). The CV plot exhibited four pairs of peaks at 1.3, 1.7, 2.3, and 2.6 V (Figure S7b). In the long term cycling test, 75.9% (131 mAh g^{-1}) of initial specific capacity with close to 100% of Coulombic efficiency was retained after 100 cycles at 50 mA g^{-1} (Figure S7c). The rate performance of the PTAD cathode in KIBs is shown in Figure S7d. The current densities of the KIB rate performance were set the same as those in NIBs. When the current density was returned to 50 mA g^{-1}, the specific capacity was recovered to 134.9 mAh g^{-1}. The PTAD cathode exhibited high capacity, long cycle life, and fast rate capability in KIBs, representing a promising polymer cathode for alkali-ion batteries.

To gain insight into the high performance of the PTAD cathode, further investigation of reaction kinetics is conducted through CV at various current densities, Randles−Sevcik analysis, electrochemical impedance spectroscopy (EIS), and the galvanostatic intermittent titration technique (GITT). To assess the polarization of the PTAD cathode in NIBs, CV tests were performed under scan rates from 0.1 to 1.0 mV s^{-1} (Figure 3a). The cathodic and anodic peaks exhibited slight shifts as the scan rates increased from 0.1 to 1.0 mV s^{-1}, indicating that PTAD does not undergo significant polarization with increased scan rates. The anodic peak at 2.2 V and the cathodic peak at 2.1 V were used to construct the Randles−Sevcik plot (Figure 3b). According to the Randles−Sevcik equation, the slope values for the cathodic and anodic peaks are 0.7928 and 0.7651, respectively. A slope value close to 1 suggests that the redox reaction is controlled by surface reaction and pseudocapacitive behavior, while a slope close to 0.5 indicates diffusion-controlled kinetics. Since the slope values for PTAD fall in the middle of 0.5 and 1, it suggests that reaction kinetics are influenced by both surface reaction and diffusion.[33,34] To further understand the reaction kinetics, GITT was performed at a current density of 50 mA g^{-1}. In Figure 3c, specific capacities of discharge and charge curves at 50 mA g^{-1} are 190.89 mAh g^{-1} and 222.09 mAh g^{-1}, respectively. Small overpotentials were observed during charge and discharge in GITT, demonstrating fast reaction kinetics.[35−37] To analyze the interfacial impedance between the PTAD electrode and electrolyte, EIS was employed. The depressed semicircle and curved line in the Nyquist plot indicate the interfacial and diffusion impedances. The interfacial impedance of the pristine electrode was 8.39 ohm. After the first cycle, the interfacial impedance was decreased to 7.07 ohm, and it was stabilized at 9.12 ohm after 50 cycles. This result indicates that a stable cathode electrolyte interphase (CEI) layer was constructed on the PTAD cathode. The low interfacial impedance and stable CEI are crucial for enabling the fast-charging capability and high cyclic stability of the PTAD cathode in NIBs. Therefore, the results from CV,

https://doi.org/10.1021/acsnano.3c08860
ACS Nano XXXX, XXX, XXX−XXX

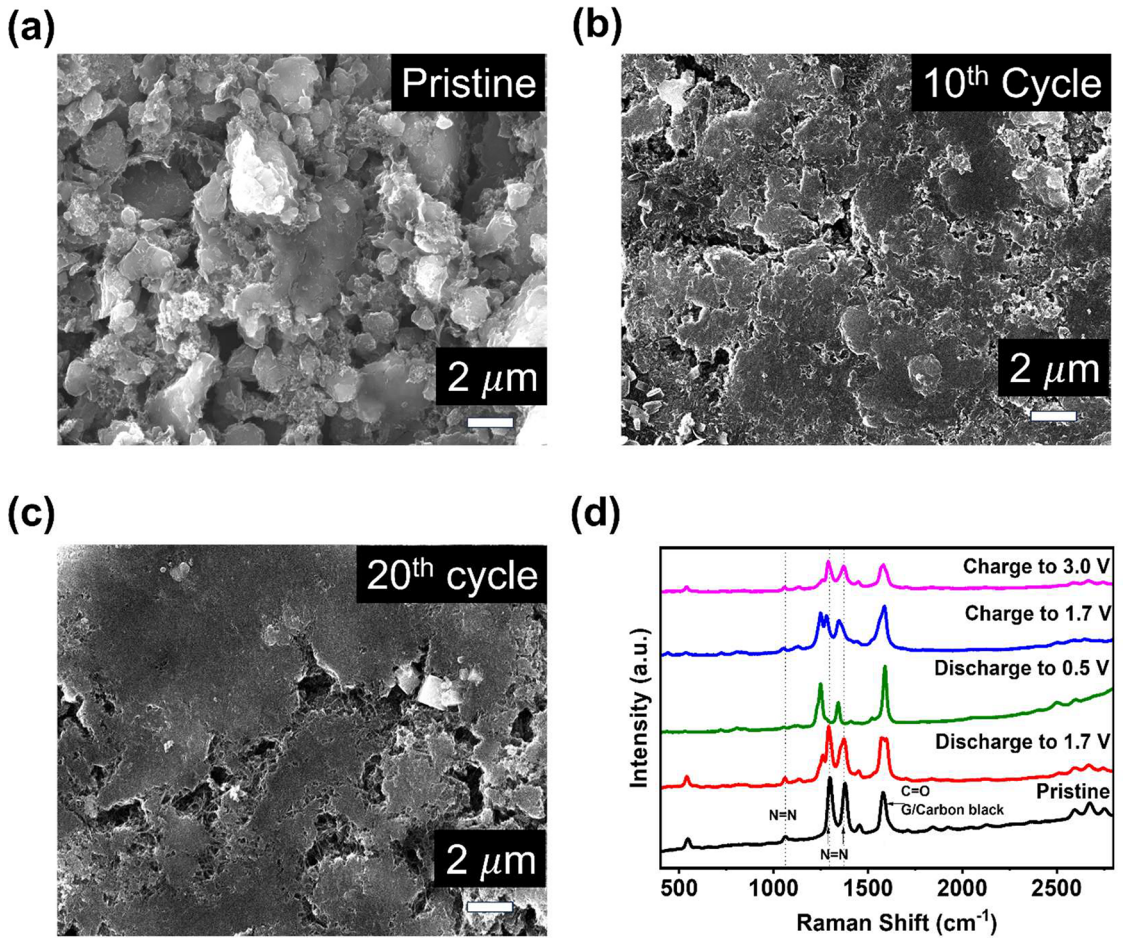

Figure 5. PTAD cathode characterization before and after cycling: SEM images of (a) the pristine, PTAD cathode surface, and cycled PTAD cathodes after (b) 10th, (c) 20th, and (d) Raman spectra at different charge and discharge stages.

EIS, and GITT collectively confirm the rapid kinetics of the PTAD cathode in NIBs.

Since the PTAD cathode exhibited superior electrochemical performance in NIBs at room temperature, we further investigated its performance at low temperatures from 0 °C to −50 °C. Galvanostatic charge−discharge curves at various testing temperatures are displayed in Figure 4a. The redox plateaus at low temperatures resembled those at room temperature, and the specific capacity at room temperature was 195.6 mAh g^{-1} at 50 mA g^{-1} (Figure S8). When the temperature was lowered to 0 °C, the specific capacity was retained at 173.1 mAh g^{-1}. Even at −50 °C, the specific capacity was still retained at 137.1 mAh g^{-1}. The decrease in the capacity is due to slower reaction kinetics at low temperatures. Upon returning to room temperature, the specific capacity was recovered to 179.4 mAh g^{-1}, corresponding to 91.8% of initial room temperature capacity (Figure 4b). The small capacity loss (−8.2%) after return from −50 °C to room temperature is probably due to the shuttle reaction caused by the low-molecular-weight PTAD polymer as evidenced by the high Coulombic efficiency of >100% in the initial cycles. In the room-temperature cyclic stability test (figure S8b), the PTAD cathode exhibits a similar capacity loss in the initial 10 cycles at 50 mA g^{-1}. After 10 cycles, the reversible capacity of the PTAD cathode is stable. This is coincident with the capacity loss after 40 cycles in the low-temperature battery test shown in Figure 4b. To further assess the long-term cycling performance of the PTAD cathode at low temperatures, it was cycled at 50 mA g^{-1} and −50 °C. The charge−discharge curves at −50 °C (Figure 4c) resembled those at room temperatures (Figure S8a). In Figure 4c, the galvanostatic charge−discharge test was started at −50 °C. Due to the low testing temperature, reaction kinetics were slow, and there was an activation process to achieve full utilization of the active material in the initial cycles. The reversible capacity gradually increases in the initial five cycles. However, in the various temperature tests (Figure 4a,b), the galvanostatic charge−discharge test was started at room temperature, and then the temperature was slowly decreased to 0 °C, −10 °C, −20 °C, −30 °C, −40 °C, and −50 °C after five cycles at each temperature. The initial test at room temperature avoids the activation process. Therefore, the first cycle for the various temperature test did not exhibit low specific capacity. To further confirm the results at −50 °C in Figure 4c, we repeated the cyclic stability test at a low temperature (−50 °C) and obtained similar results in the first cycle as shown in Figure S9. At −50 °C, the PTAD cathode retained a specific capacity of 133 mAh g^{-1} with a Coulombic efficiency close to 100% for 150 cycles (Figure 4d), demonstrating high cyclic stability at a low temperature. These results confirm that coupling the polymer cathode with a low-concentration electrolyte is an effective approach to developing low-temperature NIBs.

https://doi.org/10.1021/acsnano.3c08860
ACS Nano XXXX, XXX, XXX−XXX

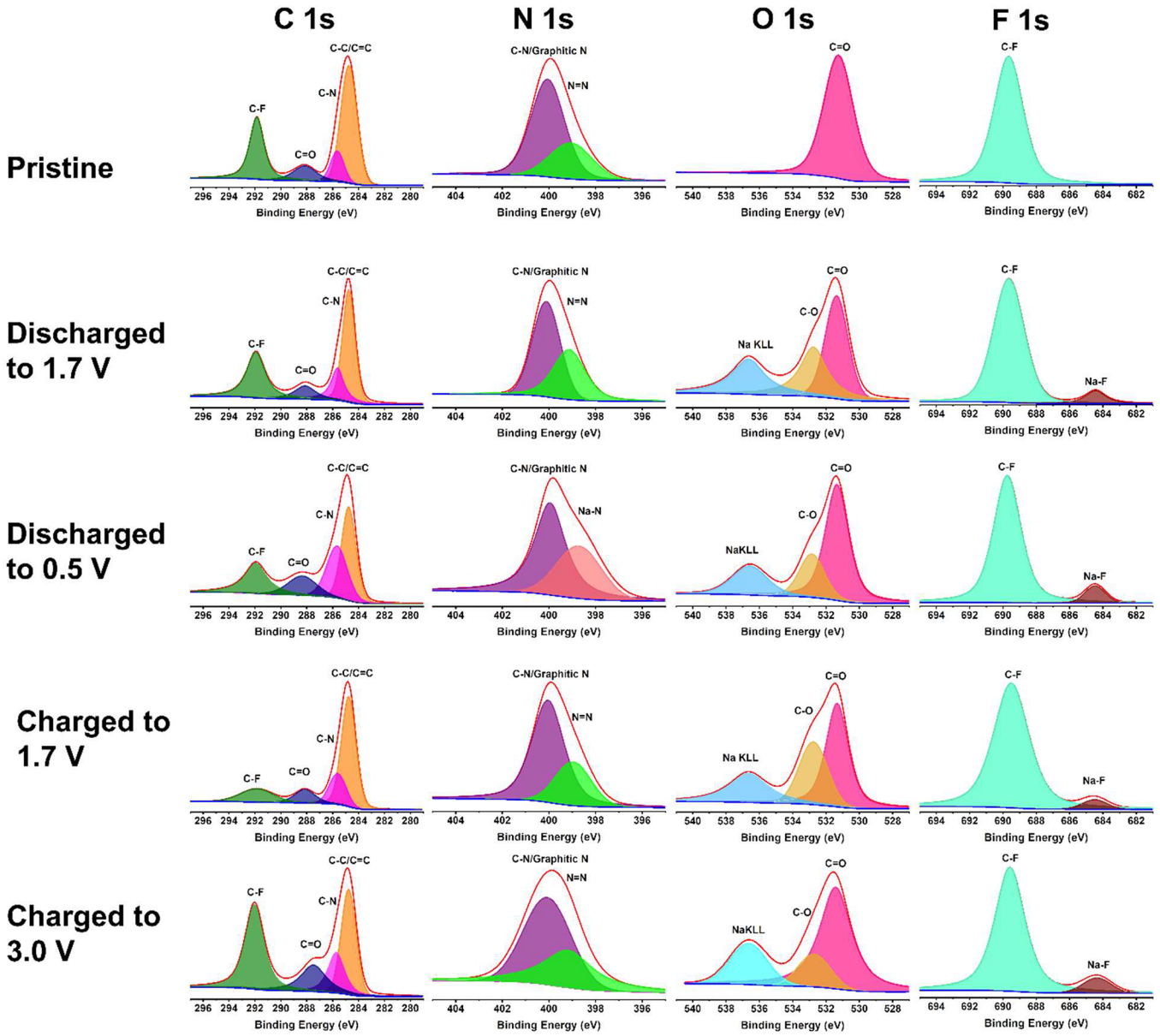

Figure 6. C 1s, N 1s, O 1s, and F 1s XPS spectra for the PTAD cathodes at various charge and discharge stages.

Given the exceptional performance of the PTAD cathode in NIBs at both room and low temperatures, SEM, Raman spectroscopy, and XPS were employed to gain insight into the morphology, reaction mechanism, and interfacial chemistry. SEM images in Figure 5a–c represent the pristine PTAD cathode and cycled PTAD cathodes after 10 and 20 cycles. No obvious cracks or particle pulverization were observed after cycling, demonstrating high structure integrity of the PTAD cathode. In the *ex situ* Raman results (Figure 5d), the azo peaks at 1060, 1300.6, and 1378 cm^{-1} for pristine PTAD disappeared when discharged to 0.5 V. New Raman peaks at 1248.39 and 1342.77 cm^{-1} appeared at 0.5 V, representing the sodiated azo group. After the PTAD cathode was charged back to 3.0 V, the azo peaks were recovered, demonstrating a reversible redox reaction between the azo group and the Na ions/electrons in NIBs. The Raman peaks corresponding to carbonyl groups in PTAD were overlapped with the peak for the graphitic carbon (G band) of carbon black at 1579 cm^{-1}, resulting in no apparent change upon cycling.[38]

To further investigate the reaction mechanism and interfacial chemistry, XPS was employed (Figure 6). The reference peak of graphitic carbon (C–C/C=C) was calibrated at 284.8 eV in the C 1s XPS spectra. The XPS peak at 291.9 eV corresponds to the C–F bond originating from the polytetrafluoroethylene (PTFE) binder. The peak of the carbonyl (C=O) bond in the imide moiety exhibited low intensity at 287.8 eV, and the peak for C–N was detected at 285.5 eV. In the N 1s spectra, the graphitic N peak was detected at 400.1 eV, and the azo (N=N) peak was observed at 399.0 eV in the pristine electrode. When PTAD was fully discharged to 0.5 V, the azo peak disappeared, and a new peak emerged at 398.4 eV, corresponding to the N–Na bond. After being charged to 1.7 V, the N–Na peak disappeared, and the azo peak was recovered, demonstrating the reversible reaction between azo groups and Na ions. In the O 1s spectrum of the pristine electrode, only the carbonyl (C=O) peak was present at 531.7 eV. After being discharged to 1.7 V, two new peaks appeared at 532.7 and 536.6 eV, representing the C–O bond

https://doi.org/10.1021/acsnano.3c08860
ACS Nano XXXX, XXX, XXX–XXX

and Na KLL. The peak intensity for the C−O bond was increased when discharged to 0.5 V, and it was decreased when charged back to 3 V, demonstrating the reversible reaction between carbonyl groups and Na ions. In F 1s spectra, the peak for the Na−F bond appeared after discharge, and it is retained during discharge and charge, demonstrating the formation of Na−F in the interphase of the PTAD cathode. Since NaF has high mechanical strength and is stable upon cycling, a NaF-rich interphase benefits the high cyclic stability and structure integrity of the PTAD cathode in NIBs.[29,39,40]

CONCLUSIONS

In summary, PTAD, composed of carbonyl and azo groups with extended conjugation structures in the repeating unit, was employed as a polymer cathode in room- and low-temperature NIBs. The carbonyl and azo groups act as active centers in PTAD, enabling multistep reversible reactions with Na^+ ions and electrons, thereby resulting in a high reversible capacity. The extended conjugation structure in PTAD enables $\pi-\pi$ stacking between NGr and the polymer, enhancing the conductivity and stability of the PTAD cathode. The PTAD cathode demonstrated a high performance, including a high reversible capacity of 206.7 mAh g^{-1} at 50 mA g^{-1}, an extended lifespan of 1500 cycles, and fast-charging capability up to 10 A g^{-1} in NIBs at room temperature. This exceptional performance was also extended to KIBs at room temperature in terms of high capacity, long cycle life, and fast-charging capability. Moreover, when combined with a low-concentration electrolyte, the PTAD cathode exhibits exceptional performance in NIBs at low temperatures from 0 to −50 °C, demonstrating significant potential for low-temperature battery applications. The reaction mechanism and interfacial chemistry of the PTAD cathode were investigated using Raman spectroscopy and XPS, confirming the redox reactions between azo/carbonyl groups and Na^+ ions/electrons, as well as the formation of a NaF-rich interphase. Therefore, this work demonstrates an effective approach to developing low-temperature NIBs through the design of bifunctional polymer cathode materials and low-concentration electrolytes.

METHODS/EXPERIMENTAL

Synthesis of PTAD. The PTAD polymer was synthesized using a polycondensation method. 1.1770 g of perylenetetracarboxylic dianhydride (98%) and 20 g of imidazole (>99.5%) were transferred into a 50 mL double-necked round-bottom flask. The flask was heated under a nitrogen atmosphere until the temperature of the oil bath reached 150 °C. The solid materials turned into a solution at that temperature. 0.6115 g of 4,4′-azodianiline (>95%) was slowly added to the flask, and the solution was stirred under a nitrogen atmosphere. The temperature of the oil bath was increased to 170 °C and maintained for 24 h. Subsequently, the temperature was reduced to 60 °C, leading to solidification of the solution. To dissolve the solidified solution, 25 mL of methanol was slowly injected into the flask. When all solid particles disappeared, the temperature was lowered to 25 °C. The solution was filtrated, and dark red precipitates were washed by centrifugation with dimethylformamide (99.8%) and ethanol, respectively. The collected powder was dried at 80 °C in a vacuum oven, yielding 85.7%.

ASSOCIATED CONTENT

Data Availability Statement

The data that support the findings of this study are available from the corresponding author upon reasonable request.

Supporting Information

The Supporting Information is available free of charge at https://pubs.acs.org/doi/10.1021/acsnano.3c08860.

Experimental methods, including synthesis of the PTAD polymer, preparing of the electrolyte, and temperature setup; pictures for the solubility test of raw-PTAD material in THF solvents (Figure S1); pictures of the freezing test of different concentrations of electrolyte (Figure S2); cyclic voltammogram of a low-concentration electrolyte (Figure S3); solubility test for the PTAD electrode in the electrolyte and electrolyte solvent (Figure S4); electrochemical performance of the PTAD cathode without NGr in NIBs and graphene electrode in NIBs (Figure S5); cyclic voltammetry of the PTAD cathode with and without NGr (Figure S6); electrochemical performance of the PTAD cathode in KIBs (Figure S7); performance of the PTAD cathode in NIBs at 50 mA g^{-1} and room temperature (Figure S8); electrochemical performances of PTAD cathodes in NIB at a low temperature (−50 °C) (Figure S9); electrochemical performances of PTAD cathodes in NIBs at room temperature (Figure S10) (PDF)

AUTHOR INFORMATION

Corresponding Author

Chao Luo − *Department of Chemistry and Biochemistry and Quantum Science and Engineering Center, George Mason University, Fairfax, Virginia 22030, United States; Department of Chemical, Environmental, and Materials Engineering, University of Miami, Coral Gables, Florida 33146, United States;* orcid.org/0000-0001-8497-8548; Email: cxl1763@miami.edu

Authors

Eric Youngsam Kim − *Department of Chemistry and Biochemistry, George Mason University, Fairfax, Virginia 22030, United States*

Motahareh Mohammadiroudbari − *Department of Chemistry and Biochemistry, George Mason University, Fairfax, Virginia 22030, United States*

Fu Chen − *Department of Chemistry and Biochemistry, University of Maryland, College Park, Maryland 20742, United States*

Zhenzhen Yang − *Chemical Sciences and Engineering Division, Argonne National Laboratory, Lemont, Illinois 60439, United States;* orcid.org/0000-0002-1073-3799

Complete contact information is available at: https://pubs.acs.org/10.1021/acsnano.3c08860

Notes

The authors declare no competing financial interest.

ACKNOWLEDGMENTS

This work was supported by the U.S. National Science Foundation Award No. 2000102. The authors also acknowledge the support from the George Mason University Quantum Science and Engineering Center. We gratefully acknowledge support from the Post Test Facility at Argonne National Laboratory, which is operated for the DOE Vehicle Technologies Office (VTO) by UChicago Argonne, LLC, under contract number DE-AC02-06CH11357. We thank the

NSF (NSF-1726058) for funding a solid-state NMR spectrometer at the University of Maryland, College Park.

REFERENCES

(1) He, Y.; Matthews, B.; Wang, J.; Song, L.; Wang, X.; Wu, G. Innovation and Challenges in Materials Design for Flexible Rechargeable Batteries: From 1D to 3D. *J. Mater. Chem. A Mater.* **2018**, *6* (3), 735−753.

(2) Zhang, H.; Gao, Y.; Liu, X.; Yang, Z.; He, X.; Li, L.; Qiao, Y.; Chen, W.; Zeng, R.; Wang, Y.; Chou, S. Organic Cathode Materials for Sodium-Ion Batteries: From Fundamental Research to Potential Commercial Application. *Adv. Funct Mater.* **2022**, *32* (4), No. 2107718.

(3) Mohammadiroudbari, M.; Qin, K.; Luo, C. Multi-Functionalized Polymers as Organic Cathodes for Sustainable Sodium/Potassium-Ion Batteries. *Batter Supercaps* **2022**, *5* (6), No. e202200021.

(4) Winslow, K. M.; Laux, S. J.; Townsend, T. G. A Review on the Growing Concern and Potential Management Strategies of Waste Lithium-Ion Batteries. *Resour. Conserv. Recycl.* **2018**, *129*, 263−277.

(5) Eftekhari, A. On the Theoretical Capacity/Energy of Lithium Batteries and Their Counterparts. *ACS Sustain Chem. Eng.* **2019**, *7* (4), 3684−3687.

(6) Li, X.; Sun, X.; Hu, X.; Fan, F.; Cai, S.; Zheng, C.; Stucky, G. D. Review on Comprehending and Enhancing the Initial Coulombic Efficiency of Anode Materials in Lithium-Ion/Sodium-Ion Batteries. *Nano Energy* **2020**, *77*, No. 105143.

(7) Kim, T.; Song, W.; Son, D.-Y.; Ono, L. K.; Qi, Y. Lithium-Ion Batteries: Outlook on Present, Future, and Hybridized Technologies. *J. Mater. Chem. A Mater.* **2019**, *7* (7), 2942−2964.

(8) Goikolea, E.; Palomares, V.; Wang, S.; de Larramendi, I. R.; Guo, X.; Wang, G.; Rojo, T. Na-Ion Batteries—Approaching Old and New Challenges. *Adv. Energy Mater.* **2020**, *10* (44), No. 2002055.

(9) Hwang, J.-Y.; Myung, S.-T.; Sun, Y.-K. Sodium-Ion Batteries: Present and Future. *Chem. Soc. Rev.* **2017**, *46* (12), 3529−3614.

(10) Holguin, K.; Mohammadiroudbari, M.; Qin, K.; Luo, C. Organic Electrode Materials for Non-Aqueous, Aqueous, and All-Solid-State Na-Ion Batteries. *J. Mater. Chem. A Mater.* **2021**, *9* (35), 19083−19115.

(11) Hubble, D.; Brown, D. E.; Zhao, Y.; Fang, C.; Lau, J.; McCloskey, B. D.; Liu, G. Liquid Electrolyte Development for Low-Temperature Lithium-Ion Batteries. *Energy Environ. Sci.* **2022**, *15* (2), 550−578.

(12) Li, Q.; Liu, G.; Cheng, H.; Sun, Q.; Zhang, J.; Ming, J. Low-Temperature Electrolyte Design for Lithium-Ion Batteries: Prospect and Challenges. *Chem. Eur. J.* **2021**, *27* (64), 15842−15865.

(13) Holoubek, J.; Yu, M.; Yu, S.; Li, M.; Wu, Z.; Xia, D.; Bhaladhare, P.; Gonzalez, M. S.; Pascal, T. A.; Liu, P.; Chen, Z. An All-Fluorinated Ester Electrolyte for Stable High-Voltage Li Metal Batteries Capable of Ultra-Low-Temperature Operation. *ACS Energy Lett.* **2020**, *5* (5), 1438−1447.

(14) Yin, L.; Wang, M.; Xie, C.; Yang, C.; Han, J.; You, Y. High-Voltage Cyclic Ether-Based Electrolytes for Low-Temperature Sodium-Ion Batteries. *ACS Appl. Mater. Interfaces* **2023**, *15* (7), 9517−9523.

(15) Wang, C.; Thenuwara, A. C.; Luo, J.; Shetty, P. P.; McDowell, M. T.; Zhu, H.; Posada-Pérez, S.; Xiong, H.; Hautier, G.; Li, W. Extending the Low-Temperature Operation of Sodium Metal Batteries Combining Linear and Cyclic Ether-Based Electrolyte Solutions. *Nat. Commun.* **2022**, *13* (1), 4934.

(16) Peng, J.; Zhang, W.; Hu, Z.; Zhao, L.; Wu, C.; Peleckis, G.; Gu, Q.; Wang, J.-Z.; Liu, H. K.; Dou, S. X.; Chou, S. Ice-Assisted Synthesis of Highly Crystallized Prussian Blue Analogues for All-Climate and Long-Calendar-Life Sodium Ion Batteries. *Nano Lett.* **2022**, *22* (3), 1302−1310.

(17) Yang, D.; Xu, J.; Liao, X.-Z.; He, Y.-S.; Liu, H.; Ma, Z.-F. Structure Optimization of Prussian Blue Analogue Cathode Materials for Advanced Sodium Ion Batteries. *Chem. Commun.* **2014**, *50* (87), 13377−13380.

(18) Qian, J.; Wu, C.; Cao, Y.; Ma, Z.; Huang, Y.; Ai, X.; Yang, H. Prussian Blue Cathode Materials for Sodium-Ion Batteries and Other Ion Batteries. *Adv. Energy Mater.* **2018**, *8* (17), No. 1702619.

(19) Peng, J.; Zhang, W.; Liu, Q.; Wang, J.; Chou, S.; Liu, H.; Dou, S. Prussian Blue Analogues for Sodium-Ion Batteries: Past, Present, and Future. *Adv. Mater.* **2022**, *34* (15), No. e202303953.

(20) Jaguemont, J.; Boulon, L.; Dubé, Y. A Comprehensive Review of Lithium-Ion Batteries Used in Hybrid and Electric Vehicles at Cold Temperatures. *Appl. Energy* **2016**, *164*, 99−114.

(21) Hubble, D.; Brown, D. E.; Zhao, Y.; Fang, C.; Lau, J.; McCloskey, B. D.; Liu, G. Liquid Electrolyte Development for Low-Temperature Lithium-Ion Batteries. *Energy Environ. Sci.* **2022**, *15* (2), 550−578.

(22) Zhao, Q.; Lu, Y.; Chen, J. Advanced Organic Electrode Materials for Rechargeable Sodium-Ion Batteries. *Adv. Energy Mater.* **2017**, *7* (8), No. 1601792.

(23) Lee, D. H.; Xu, J.; Meng, Y. S. An Advanced Cathode for Na-Ion Batteries with High Rate and Excellent Structural Stability. *Phys. Chem. Chem. Phys.* **2013**, *15* (9), 3304.

(24) Li, P.; Hu, N.; Wang, J.; Wang, S.; Deng, W. Recent Progress and Perspective: Na Ion Batteries Used at Low Temperatures. *Nanomaterials* **2022**, *12* (19), 3529.

(25) Nie, P.; Shen, L.; Pang, G.; Zhu, Y.; Xu, G.; Qing, Y.; Dou, H.; Zhang, X. Flexible Metal−Organic Frameworks as Superior Cathodes for Rechargeable Sodium-Ion Batteries. *J. Mater. Chem. A* **2015**, *3* (32), 16590−16597.

(26) Li, Z.; Zhang, Y.; Zhang, J.; Cao, Y.; Chen, J.; Liu, H.; Wang, Y. Sodium-Ion Battery with a Wide Operation-Temperature Range from − 70 to 100 °C. *Angew. Chem., Int. Ed.* **2022**, *61* (13), No. e202116930.

(27) Chen, J.; Peng, Y.; Yin, Y.; Fang, Z.; Cao, Y.; Wang, Y.; Dong, X.; Xia, Y. A Desolvation-Free Sodium Dual-Ion Chemistry for High Power Density and Extremely Low Temperature. *Angew. Chem., Int. Ed.* **2021**, *60* (44), 23858−23862.

(28) Shea, J. J.; Luo, C. Organic Electrode Materials for Metal Ion Batteries. *ACS Appl. Mater. Interfaces* **2020**, *12* (5), 5361−5380.

(29) Mohammadiroudbari, M.; Huang, J.; Kim, E. Y.; Yang, Z.; Chen, F.; Luo, C. Porous Bipolar Polymers as Organic Cathodes for Sustainable Sodium/Potassium-Ion Batteries. *J. Mater. Chem. A* **2023**, *11* (31), 16636−16647.

(30) Mohammadiroudbari, M.; Qin, K.; Luo, C. Multi-Functionalized Polymers as Organic Cathodes for Sustainable Sodium/Potassium-Ion Batteries. *Batter Supercaps* **2022**, *5* (6), No. e202200021.

(31) Pang, W.; Xue, J.; Pang, H. A High Energy Density Azobenzene/Graphene Oxide Hybrid with Weak Nonbonding Interactions for Solar Thermal Storage. *Sci. Rep* **2019**, *9* (1), No. 5224.

(32) Thorn, K. A. 13C and 15N NMR Identification of Product Compound Classes from Aqueous and Solid Phase Photodegradation of 2,4,6-Trinitrotoluene. *PLoS One* **2019**, *14* (10), No. e0224112.

(33) Kim, T.; Choi, W.; Shin, H.-C.; Choi, J.-Y.; Kim, J. M.; Park, M.-S.; Yoon, W.-S. Applications of Voltammetry in Lithium Ion Battery Research. *J. Electrochem. Sci. Technol.* **2020**, *11* (1), 14−25.

(34) Ottmann, A.; Zakharova, G. S.; Ehrstein, B.; Klingeler, R. Electrochemical Performance of Single Crystal Belt-like NH4V3O8 as Cathode Material for Lithium-Ion Batteries. *Electrochim. Acta* **2015**, *174*, 682−687.

(35) Li, Z.; Du, F.; Bie, X.; Zhang, D.; Cai, Y.; Cui, X.; Wang, C.; Chen, G.; Wei, Y. Electrochemical Kinetics of the Li[Li $_{0.23}$ Co $_{0.3}$ Mn $_{0.47}$]O $_2$ Cathode Material Studied by GITT and EIS. *J. Phys. Chem. C* **2010**, *114* (51), 22751−22757.

(36) Nickol, A.; Schied, T.; Heubner, C.; Schneider, M.; Michaelis, A.; Bobeth, M.; Cuniberti, G. GITT Analysis of Lithium Insertion Cathodes for Determining the Lithium Diffusion Coefficient at Low Temperature: Challenges and Pitfalls. *J. Electrochem. Soc.* **2020**, *167* (9), No. 090546.

(37) Dees, D. W.; Kawauchi, S.; Abraham, D. P.; Prakash, J. Analysis of the Galvanostatic Intermittent Titration Technique (GITT) as

https://doi.org/10.1021/acsnano.3c08860
ACS Nano XXXX, XXX, XXX−XXX

Applied to a Lithium-Ion Porous Electrode. *J. Power Sources* **2009**, *189* (1), 263−268.
(38) Zafar, Z.; Ni, Z. H.; Wu, X.; Shi, Z. X.; Nan, H. Y.; Bai, J.; Sun, L. T. Evolution of Raman Spectra in Nitrogen Doped Graphene. *Carbon* **2013**, *61*, 57−62.
(39) Qin, K.; Tan, S.; Mohammadiroudbari, M.; Yang, Z.; Yang, X. Q.; Hu, E.; Luo, C. Synergy of Carbonyl and Azo Chemistries for Wide-Temperature-Range Rechargeable Aluminum Organic Batteries. *Nano Energy* **2022**, *101*, No. 107554.
(40) Wang, Y.; Yu, J.; Peng, W.; Tian, J.; Yang, C. Novel Multilayer TiO2 Heterojunction Decorated by Low G-C3N4 Content and Its Enhanced Photocatalytic Activity under UV, Visible and Solar Light Irradiation. *Sci. Rep* **2019**, *9* (1), 5932.
(41) Cao, M.; Fu, A.; Wang, Z.; Liu, J.; Kong, N.; Zong, H.; Liu; Gooding, J. J. Electrochemical and theoretical study of $\pi-\pi$ Stacking Interactions between Graphitic Surfaces and Pyrene Derivatives. *J. Phys. Chem. C* **2014**, *118* (5), 2650−2659.
(42) Zhang, C.; Cheng, J.; Wu, Q.; Hou, S.; Feng, S.; Jiang, B.; Lambert, C. J.; Gao, X.; Li, Y.; Li, J. Enhanced $\pi-\pi$ Stacking between Dipole−Bearing Single Molecules Revealed by Conductance Measurement. *J. Am. Chem. Soc.* **2023**, *145* (3), 1617−1630.
(43) Tang, M.; Zhu, S.; Liu, Z.; Jiang, C.; Wu, Y.; Li, H.; Wang, B.; Wang, E.; Ma, J.; Wang, C. Tailoring π−Conjugated Systems: From $\pi-\pi$ Stacking to High-Rate-Performance Organic Cathodes. *Cell Press Chem.* **2018**, *4* (11), 2600−2614.

https://doi.org/10.1021/acsnano.3c08860
ACS Nano XXXX, XXX, XXX−XXX